$$\boldsymbol{Q}_V = \sum_e \int_{Ve} \boldsymbol{B}^{\mathrm{T}} \boldsymbol{S}_V dV, \qquad (A2.10)$$

$$\boldsymbol{H} = \sum_e \int_{Ve} \boldsymbol{B}^{\mathrm{T}} \boldsymbol{D}_c \boldsymbol{N}_\lambda dV, \qquad (A2.11)$$

$$\boldsymbol{F}_S = \sum_e \int_{Se} \boldsymbol{N}_u^{\mathrm{T}} \bar{\boldsymbol{t}} dS, \qquad (A2.12)$$

$$\boldsymbol{\Gamma} = \sum_e \int_{Ve} \boldsymbol{N}_\lambda^{\mathrm{T}} \boldsymbol{N}_\lambda dV, \qquad (A2.13)$$

$$\boldsymbol{\Psi} = \sum_e \int_{Ve} \Psi \boldsymbol{N}_\lambda^{\mathrm{T}} dV. \qquad (A2.14)$$

In the above equations, $\boldsymbol{N}_u$ and $\boldsymbol{N}_\lambda$ are the matrix and the vector consisting of the interpolation functions of $\boldsymbol{u}$ and λ, respectively. Ve and Se represent the subdomains of each finite element. $\sum_e$ indicates the element assemblage. $\boldsymbol{U}$ and $\boldsymbol{\Lambda}$ are vectors aligning the discretized values of $\boldsymbol{u}$ and λ at all nodes, respectively. $\ddot{}$ indicates the second-order time derivative. Starting from the left, the terms in Equation A2.7 are the inertial force, internal force, hydrostatic pressure, and external force.

Using the central difference method with a time increment of Δt, we decompose Equation A2.7 as follows:

$$\boldsymbol{M}^{t+\Delta t}\ddot{\boldsymbol{U}} = \Delta t^2 \left({}^{t+\Delta t}\boldsymbol{F}_S - {}^{t+\Delta t}\boldsymbol{Q}_V - {}^{t+\Delta t}\boldsymbol{H}\,{}^{t+\Delta t}\boldsymbol{\Lambda} \right) + \boldsymbol{M}(2{}^{t}\boldsymbol{U} - {}^{t-\Delta t}\boldsymbol{U}) \qquad (A2.15)$$

where left superscripts represent times. We use the inertial force at time t and other forces at time $t + \Delta t$.

We solved Equation A2.15 with Equation A2.8 iteratively, as follows, to get ${}^{t+\Delta t}\boldsymbol{U}$ and ${}^{t+\Delta t}\boldsymbol{\Lambda}$.

Using the intermediate variable, $\boldsymbol{U}_m$, we decoupled Equation A2.15 as follows:

$$\boldsymbol{M}_{k+1}\boldsymbol{U}_m = \Delta t^2 \left({}^{t+\Delta t}\boldsymbol{F}_S - {}^{t+\Delta t}_{k+1}\boldsymbol{Q}_V \right) + \boldsymbol{M}(2{}^{t}\boldsymbol{U} - {}^{t-\Delta t}\boldsymbol{U}) \qquad (A2.16)$$

$$\boldsymbol{M}\left({}^{t+\Delta t}_{k+1}\boldsymbol{U} - {}_{k+1}\boldsymbol{U}_m \right) = -\Delta t^2\, {}^{t+\Delta t}_{k+1}\boldsymbol{H}\, {}^{t+\Delta t}_{k+1}\boldsymbol{\Lambda}, \qquad (A2.17)$$

where left subscripts, $k + 1$, represent the $(k + 1)$th iteration.

Variations in Ψ and $\delta\Psi$ due to $\delta\boldsymbol{u}$ can be written as follows:

$$\delta\Psi = (\partial\Psi/\partial C_{ij})\delta C_{ij} = 1/2\boldsymbol{D}_C^{\mathrm{T}}\{\delta\boldsymbol{C}\} = \boldsymbol{D}_C^{\mathrm{T}}\boldsymbol{B}\{\delta\boldsymbol{u}\}. \qquad (A2.18)$$

Then, $\delta\boldsymbol{\Psi}$, the variation of $\boldsymbol{\Psi}$ due to $\delta\boldsymbol{u}$, can be written as follows:

$$\delta\boldsymbol{\Psi} = \sum_e \int_{Ve} \boldsymbol{N}_\lambda^{\mathrm{T}} \boldsymbol{D}_C^{\mathrm{T}} \boldsymbol{B}\,\{\delta\boldsymbol{u}\}\, dV = \boldsymbol{H}^{\mathrm{T}}\delta\boldsymbol{U} \qquad (A2.19)$$

where $\delta\boldsymbol{U}$ is the variation of $\boldsymbol{U}$.

Therefore, Equation A2.8 at time $t + \Delta t$ can be written as follows:

$$(1/\alpha)\, {}^{t+\Delta t}_{k+1}\boldsymbol{\Gamma}\, {}^{t+\Delta t}_{k+1}\boldsymbol{\Lambda} = {}^{t+\Delta t}_{k+1}\boldsymbol{\Psi} = {}^{t+\Delta t}_{k}\boldsymbol{\Psi} + {}^{t+\Delta t}_{k}\boldsymbol{H}^{\mathrm{T}}\left({}^{t+\Delta t}_{k+1}\boldsymbol{U} - {}^{t+\Delta t}_{k}\boldsymbol{U} \right) \qquad (A2.20)$$

From Equations A2.17 and A2.20, the following equation is obtained:

$$\left\{ (1/\alpha)^{t+\Delta t}_{k+1}\boldsymbol{\Gamma} + \Delta t^2\, {}^{t+\Delta t}_{k}\boldsymbol{H}^{\mathrm{T}}\boldsymbol{M}^{1}\, {}^{t+\Delta t}_{k+1}\boldsymbol{H}^{\mathrm{T}} \right\} {}^{t+\Delta t}_{k+1}\boldsymbol{\Lambda} = -{}^{t+\Delta t}_{k}\boldsymbol{H}^{\mathrm{T}}\left({}^{t+\Delta t}_{k}\boldsymbol{U} - {}_{k+1}\boldsymbol{U}_m \right) + {}^{t+\Delta t}_{k}\boldsymbol{\Psi} \qquad (A2.21)$$

We update $\boldsymbol{U}_{\mathrm{m}}$, ${}^{t+\Delta t}\boldsymbol{\Lambda}$, and ${}^{t+\Delta t}\boldsymbol{U}$ using Equations A2.16-A2.17, in turn, until they converge. Here, ${}^{t+\Delta t}_{k+1}\boldsymbol{Q}_V$ in Equation A2.16 and ${}^{t+\Delta t}_{k+1}\boldsymbol{H}$ in Equations A2.17 and A2.21 are functions of ${}^{t+\Delta t}_{k+1}\boldsymbol{U}$, which is unknown before Equation A2.17 is solved. Therefore, we used ${}^{t+\Delta t}_{k}\boldsymbol{Q}_V$ and ${}^{t+\Delta t}_{k}\boldsymbol{H}$ instead.

In the above procedure, we use the lumped mass matrix as $\boldsymbol{M}$. Therefore, simultaneous equations only need to be solved for ${}^{t+\Delta t}\boldsymbol{\Lambda}$ in Equation A2.21. The stability and accuracy are thus preserved while saving central processing unit time.

INTERNATIONAL JOURNAL FOR NUMERICAL METHODS IN ENGINEERING
Int. J. Numer. Meth. Engng 2009; **78**:483–504
Published online 18 November 2008 in Wiley InterScience (www.interscience.wiley.com). DOI: 10.1002/nme.2497

Development of a finite element contact analysis algorithm for charged-hydrated soft tissues with large sliding

Xian Chen[1,*,†,‡], Kenji Sunagawa[2,‡] and Toshiaki Hisada[3,‡]

[1]*Digital Medicine Initiative, Kyushu University, 3-1-1 Maidashi, Higashi-ku, Fukuoka 812-8582, Japan*
[2]*Graduate School of Medical Sciences, Kyushu University, Fukuoka, Japan*
[3]*School of Frontier Sciences, The University of Tokyo, Tokyo, Japan*

SUMMARY

This paper focuses on a finite element analysis of contact phenomena with large sliding between charged-hydrated biological soft tissues, such as articular cartilages, based on the triphasic theory. The impenetrability constraint between the contacting bodies and the continuity of the interstitial fluid and ion phases at the contact surfaces are imposed by applying a Lagrange multiplier approach with the contact pressure, chemical potential of the fluid and electrochemical potentials of ions as Lagrange multipliers. A node-to-segment one-pass approach is adopted to cope with large deformations and sliding between the contact surfaces. To pass the contact patch test, contact boundary integrations are performed on both the master and slave contact surfaces. On the other hand, the degrees of freedom of the multipliers at the master nodes are eliminated by projecting the master nodes onto the slave surface to avoid overconstraint. The effectiveness of the proposed algorithm is verified by a couple of numerical examples, in which continuous distributions of displacement, fluid flow, ionic molar flow and Lagrange multipliers on or across the contact surface are confirmed. Copyright © 2008 John Wiley & Sons, Ltd.

Received 8 June 2008; Revised 1 October 2008; Accepted 3 October 2008

KEY WORDS: finite element methods; contact problem; charged-hydrated soft tissue; patch test; cartilage

1. INTRODUCTION

In biomechanical and geomechanical fields, soft tissues, soil and clay can be characterized as charged-hydrated materials. In the case of articular cartilages in particular, the extracellular matrix (ECM) consists of complex collagen–proteoglycan solid networks and is completely saturated by interstitial water that comprises 70–85% of the weight of the cartilage. The proteoglycan

*Correspondence to: Xian Chen, Digital Medicine Initiative, Kyushu University, 3-1-1 Maidashi, Higashi-ku, Fukuoka 812-8582, Japan.
†E-mail: xchen@digital.med.kyushu-u.ac.jp
‡Professor.

Contract/grant sponsor: The Japan Society for the Promotion of Science; contract/grant number: (C) 14550067

aggregates are negatively charged by attached sulfated glycosaminoglycans with a fixed-charge density at physiologic pH. In addition, the electrolytes sodium and chloride are the dominant ions dissolved in the interstitial water [1]. This multiphasic nature of the tissue, especially the existence of fixed charges and ions, induces mechanical electrochemical coupling phenomena such as swelling, streaming potentials and electro-osmosis [2–7]. In particular, extra mechanical stresses resulting from electrochemical swelling have been revealed to play an important role in the functional load support of articular cartilages. To investigate the mechanical electrochemical coupling phenomena in charged-hydrated soft tissues, several theoretical models have been proposed, including an electromechanical model [8], a triphasic model [9], a quadriphasic model [10] and a multiphasic model [11], by assuming that the tissues are mixtures composed of a solid phase (ECM), a fluid phase (interstitial fluid) and ionic phases (cation and anion phases), and by taking the coupling behaviors between the components into account in the frameworks of continuum mechanics and electrochemistry. As analytical solutions of these theoretical models can only be obtained for quite simplified problems due to their complexities, several numerical approaches have been developed by applying the finite element method as an effective tool [12–14].

On the other hand, as a biomechanical characteristic, the contact phenomenon distinguishes articular cartilages from other soft tissues such as intervertebral disks, since diarthrodial joints function as a load transfer mechanism by contact between cartilage surfaces. This biomechanical characteristic first attracted research attention to examine the articular cartilages under the biphasic assumption by omitting the mechanical electrochemical coupling. Theoretical investigations have been carried out in the case of infinitesimal deformation [15–26]. In addition, finite element analyses have been presented without consideration of sliding between the articular cartilages [27–32]. However, contact analysis of articular cartilages without considering sliding has a significant drawback in its application because large sliding between articular cartilages in the human body actually occurs during daily life. In the framework of a finite element analysis, the contact surfaces are divided into contact segments. If the meshes of the different contact surfaces become non-conforming at the contact interface due to arbitrary mesh generation or relative sliding during deformation, the patch test represents a necessary condition for solution of the adopted contact analysis algorithm to converge toward the correct solution with mesh refinement. If a contact analysis algorithm fails in the patch test, it is inevitable that not only errors in the contact traction of the tissues, but also errors of the hydrostatic pressure and the chemical and electrochemical potentials will be induced, which further disturb solutions of the fluid and ion flow fields. Recently, biphasic finite element contact analyses considering large sliding of cartilages have been performed by Yang and Spilker [33] and Pawaskar *et al.* [34]. In the former, a specific combination of element types between the contact surfaces is needed to satisfy the requirement of the patch test, while in the latter, the analysis has been limited to the case of contact between rigid and deformable surfaces. It is worth mentioning that the biphasic finite element contact analysis algorithm developed by the authors in a previous work [35] has the ability of handling the sliding contact between deformable surfaces under large deformation, while having the robustness of passing the contact patch test for an arbitrary mesh configuration.

As the fixed negative charge content of the proteoglycan aggregates is strongly associated with the mechanical behavior of articular cartilages [36, 37], it is necessary to take the mechano-electrochemical coupling behavior into account during contact analyses of articular cartilages. Recently, theoretical studies regarding this issue have been presented [38, 39]. However, to the best of the authors' knowledge, numerical simulation of contact phenomena between deformable articular cartilage layers with mechano-electrochemical coupling and large sliding have not yet

DOI: 10.1002/nme

been reported in the literature. In this paper, attention is focused on developing a finite element contact analysis algorithm for charged-hydrated soft tissues. In the framework of the finite element formulation proposed by the authors [12] to deal with mechano-electrochemical coupling behavior based on the triphasic theory [9], the impenetrability constraint of the contacting tissues and the continuity requirements (jump conditions) derived by Ateshian *et al.* [39] and Hou *et al.* [40] for interstitial fluid and ionic phases at the contact surfaces are imposed by introducing the total stress, chemical potential of the fluid and electrochemical potentials of ions as Lagrange multipliers. Large sliding between contact surfaces is allowed in the formulation by applying a node-to-segment one-pass approach. Contact boundary integrations are performed on both the master and slave contact surfaces to pass the contact patch test, while the degrees of freedom of the multipliers at the master nodes are eliminated by projecting the master nodes onto the slave surface to avoid overconstraint.

The outline of this paper is as follows. The finite element formulation based on the triphasic theory is introduced in Section 2. The finite element contact analysis algorithm concerning the contact patch test is formulated in Section 3. Although the friction effect is omitted in this paper for the sake of simplicity, it is not difficult to extend the formulation to friction problems by applying a suitable friction law. A couple of numerical examples are presented in Section 4 to verify the effectiveness of the proposed algorithm.

2. FINITE ELEMENT FORMULATION OF THE TRIPHASIC THEORY

In the triphasic theory [9], by assuming that the cation–anion and ion–solid interactions are negligible compared with the solid–fluid and ion–fluid interactions, the quasi-static momentum equations of the tissue, fluid, cation and anion phases are given by

$$\nabla\cdot\boldsymbol{\sigma}=\mathbf{0} \tag{1}$$

$$\rho_T^{\mathrm{w}}\nabla_\mu^{\mathrm{w}}=-\boldsymbol{\kappa}^{-1}\cdot\mathbf{w}-\frac{c^+RT}{\phi^{\mathrm{w}}}\mathbf{d}^{+^{-1}}\cdot\mathbf{w}-\frac{c^-RT}{\phi^{\mathrm{w}}}\mathbf{d}^{-^{-1}}\cdot\mathbf{w}+\frac{RT}{\phi^{\mathrm{w}}}\mathbf{d}^{+^{-1}}\cdot\mathbf{j}^+ +\frac{RT}{\phi^{\mathrm{w}}}\mathbf{d}^{-^{-1}}\cdot\mathbf{j}^- \tag{2}$$

$$M^+\nabla\tilde{\mu}^+=\frac{RT}{\phi^{\mathrm{w}}}\mathbf{d}^{+^{-1}}\cdot\mathbf{w}-\frac{RT}{\tilde{c}^+}\mathbf{d}^{+^{-1}}\cdot\mathbf{j}^+ \tag{3}$$

$$M^-\nabla\tilde{\mu}^-=\frac{RT}{\phi^{\mathrm{w}}}\mathbf{d}^{-^{-1}}\cdot\mathbf{w}-\frac{RT}{\tilde{c}^-}\mathbf{d}^{-^{-1}}\cdot\mathbf{j}^- \tag{4}$$

where $\boldsymbol{\sigma}$ is the total Cauchy stress tensor of the tissue; by denoting constituent α with superscript s, w and $\pm$ for the solid, fluid and ionic phases, respectively, ρ_T^α and $\mathbf{v}^\alpha$ give the real density (true density) and velocity of each phase, respectively; the ionic molar concentration $\tilde{c}^\alpha(\alpha=+,-)$ is defined as the moles of ions per unit volume of the tissue; ϕ^{s} and ϕ^{w} are the volume fractions of the solid and fluid phases, respectively; the velocities of the fluid and ionic phases relative to the solid phase are defined as $\mathbf{w}=\phi^{\mathrm{w}}(\mathbf{v}^{\mathrm{w}}-\mathbf{v}^{\mathrm{s}})$ and $\mathbf{j}^\alpha=\tilde{c}^\alpha(\mathbf{v}^\alpha-\mathbf{v}^{\mathrm{s}})$ in the sense of the fluid and ionic molar fluxes, respectively; μ^{w}, $\tilde{\mu}^+$ and $\tilde{\mu}^-$ are the chemical potential of the fluid and the electrochemical potentials of the cation and anion phases per unit mass, respectively; $\boldsymbol{\kappa}$ and $\mathbf{d}^\alpha$ represent the permeability and ionic diffusion coefficients, respectively; R and T denote the universal gas constant and absolute temperature, respectively; $c^\alpha(\alpha=+,-)$ is the ionic molar concentration defined as the moles of ions per unit volume of interstitial water and related to $\tilde{c}^\alpha$ by

DOI: 10.1002/nme

$\tilde{c}^{\alpha}=c^{\alpha}\phi^{\mathrm{w}}$; and $M^{\alpha}(\alpha=+,-)$ denotes the ionic molecular weight related to the apparent densities of ions as $\rho^{\alpha}=c^{\alpha}\phi^{\mathrm{w}}M^{\alpha}$.

In addition, the intrinsic incompressible assumption of the solid and fluid phases leads a constraint condition in the form of:

$$\nabla\cdot(\mathbf{v}^{\mathrm{s}}+\mathbf{w})=0 \tag{5}$$

The constraint of electroneutrality due to the electroneutral requirement of the whole tissue is expressed by

$$\tilde{c}^{+}-\tilde{c}^{-}-\tilde{c}^{F}=0 \tag{6}$$

where $\tilde{c}^{F}$ is the negative fixed-charge density defined as equivalent moles per unit tissue volume with a relationship to c^{F}, defined as the equivalent moles per unit volume of interstitial water, given by $\tilde{c}^{F}=c^{F}\phi^{\mathrm{w}}$. In addition, Equation (6) can be equivalently expressed as:

$$\nabla\cdot(\mathbf{j}^{+}-\mathbf{j}^{-})=0 \tag{7}$$

Furthermore, under the assumption that the intrinsic viscosities of both the solid and fluid phases can be neglected, the total Cauchy stress for the whole tissue and the chemical and electrochemical potentials for the fluid and univalent ions are given by

$$\boldsymbol{\sigma}=-p\mathbf{I}+\boldsymbol{\sigma}^{\mathrm{e}} \tag{8}$$

$$\mu^{\mathrm{w}}=\mu_0^{\mathrm{w}}+\frac{p}{\rho_T^{\mathrm{w}}}-\frac{RT}{\rho_T^{\mathrm{w}}}\Phi(c^{+}+c^{-}) \tag{9}$$

$$\tilde{\mu}^{+}=\mu_0^{+}+\frac{RT}{M^{+}}\ln(\gamma^{+}c^{+})+\left(\frac{\eta}{M^{+}}\right) \tag{10}$$

$$\tilde{\mu}^{-}=\mu_0^{-}+\frac{RT}{M^{-}}\ln(\gamma^{-}c^{-})-\left(\frac{\eta}{M^{-}}\right) \tag{11}$$

where p is the hydrostatic pressure, $\mathbf{I}$ denotes the identity tensor, $\boldsymbol{\sigma}^{\mathrm{e}}$ is the part of the stress produced by elastic deformation of the solid matrix, $\mu_0^{\alpha}(\alpha=w,+,-)$ is the reference chemical potential of the fluid and electrochemical potentials of the ionic phases, Φ is the osmotic coefficient assumed to be the same for both ionic phases, $\gamma^{\pm}$ are the activity coefficients of the cation and anion phases and η is the product of the Faraday constant and the electric potential.

Finally, the boundary conditions are given by

$$\begin{aligned}&\boldsymbol{\sigma}\cdot\mathbf{n}=\mathbf{f}^{*}\quad\text{on }\gamma_t;\quad \mu^{\mathrm{w}}=\mu^{w*}\quad\text{on }\gamma_w\\&\tilde{\mu}^{+}=\tilde{\mu}^{+*}\quad\text{on }\gamma_+;\quad \tilde{\mu}^{-}=\tilde{\mu}^{-*}\quad\text{on }\gamma_-\end{aligned} \tag{12}$$

$$\begin{aligned}&\mathbf{u}^{\mathrm{s}}=\mathbf{u}^{\mathrm{s}*}\quad\text{on }\gamma_{us};\quad \mathbf{w}=\mathbf{w}^{*}\quad\text{on }\gamma_{jw}\\&\mathbf{j}^{+}=\mathbf{j}^{+*}\quad\text{on }\gamma_{j+};\quad \mathbf{j}^{-}=\mathbf{j}^{-^{*}}\quad\text{on }\gamma_{j-}\end{aligned} \tag{13}$$

where the superscript * indicates the prescribed boundary values, $\mathbf{n}$ is the unit outward normal vector of the surface and $\mathbf{f}^{*}$ is the traction applied on the boundary γ_t. Correspondingly, the fluid chemical potential and ionic electrochemical potentials are prescribed on the boundaries $\gamma_{\mathrm{w}}, \gamma_+$

DOI: 10.1002/nme

and γ_-, respectively. The solid displacement $\mathbf{u}^*$, fluid flux $\mathbf{w}^*$ and ionic fluxes $\mathbf{j}^{+*}$ and $\mathbf{j}^{-*}$ are specified on the boundaries $\gamma_{us}, \gamma_{jw}, \gamma_{j+}$, and γ_{j-}, respectively.

To solve the equation system including Equations (1)–(5) and (7) with the constitutive relationships in Equations (8)–(11) and boundary conditions in Equations (12)–(13) for large deformation problems in the authors' previous work [12], fluxes of the fluid and ionic phases defined in an imaginary reference configuration were introduced by applying a Piola transformation. Therefore, the divergence operator, the normal vector and the differential area in boundary conditions defined in the reference configuration were used for the convenience of their deformation independence. However, in the present work, the same fluxes defined in the current configuration are used since the continuity conditions (jump conditions) on the boundaries are given in the current configuration. In this case, the divergence operator, the normal vector and the differential area in boundary conditions are defined in the current configuration and are thus updated in accordance with deformation for large deformation problems. On the other hand, in the derivation of tangent stiffness, differentiations of the divergence operator, the normal vector and the differential area in boundary conditions with respect to the displacement are carried out by first pulling them back to the reference configuration and then pushing the results forward to the current configuration. The finite element formulation of the government equations of the triphasic theory is carried out by applying the standard weighted residual procedure. By multiplying the weight functions $\delta\mathbf{u}$ with Equation (1), $\delta\mathbf{w}$, $\delta\mathbf{j}^+$ and $\delta\mathbf{j}^-$ with Equations (2)–(4), δp with Equation (5) and $\delta\eta$ with Equation (7), respectively, and then integrating by parts the resulting equations over the volume domain of the solid phase ω, after applying the divergence theorem and transformation of the volume domain ω to the corresponding domain in the reference configuration, the weak form of the governing equations of the triphasic theory can be derived as

$$\int_\Omega \delta\mathbf{E}^{\mathrm{s}}\cdot\mathbf{S}_E^{\mathrm{s}}\,\mathrm{d}V - \int_\Omega p\nabla\cdot\delta\mathbf{u}\,\mathrm{d}V = \int_{\gamma_t}\delta\mathbf{u}\cdot\mathbf{f}^*\,\mathrm{d}s \tag{14}$$

$$\int_\Omega \nabla\cdot\delta\mathbf{w}\mu^{\mathrm{w}}J\,\mathrm{d}V - \int_\Omega \delta\mathbf{w}\cdot\left(\mathbf{k}^{-1}\cdot\mathbf{w} + c^+\frac{RT}{\phi^{\mathrm{w}}}\mathbf{d}^{+-1}\cdot\mathbf{w} + c^-\frac{RT}{\phi^{\mathrm{w}}}\mathbf{d}^{--1}\cdot\mathbf{w} - \frac{RT}{\phi^{\mathrm{w}}}\mathbf{d}^{+-1}\cdot\mathbf{j}^+ - \frac{RT}{\phi^{\mathrm{w}}}\mathbf{d}^{--1}\cdot\mathbf{j}^-\right)J\,\mathrm{d}V = \int_{\gamma_{\mathrm{w}}}\delta\mathbf{w}\cdot\mu^{\mathrm{w}^*}\mathbf{n}\,\mathrm{d}s \tag{15}$$

$$\int_\Omega \nabla\cdot\delta\mathbf{j}^+\cdot\tilde{\mu}^+J\,\mathrm{d}V + \int_\Omega \delta\mathbf{j}^+\cdot\left(\frac{RT}{\phi^{\mathrm{w}}}\mathbf{d}^{+-1}\cdot\mathbf{w} - \frac{1}{c^+}\frac{RT}{\phi^{\mathrm{w}}}\mathbf{d}^{+-1}\cdot\mathbf{j}^+\right)J\,\mathrm{d}V = \int_{\gamma_+}\delta\mathbf{j}^+\cdot\tilde{\mu}^{+*}\mathbf{n}\,\mathrm{d}s \tag{16}$$

$$\int_\Omega \nabla\cdot\delta\mathbf{j}^-\cdot\tilde{\mu}^-J\,\mathrm{d}V + \int_\Omega \delta\mathbf{j}^-\cdot\left(\frac{RT}{\phi^{\mathrm{w}}}\mathbf{d}^{--1}\cdot\mathbf{w} - \frac{1}{c^-}\frac{RT}{\phi^{\mathrm{w}}}\mathbf{d}^{--1}\cdot\mathbf{j}^-\right)J\,\mathrm{d}V = \int_{\gamma_-}\delta\mathbf{j}^-\cdot\tilde{\mu}^{-*}\mathbf{n}\,\mathrm{d}s \tag{17}$$

$$\int_\Omega \delta p\cdot\nabla\cdot(\mathbf{v}^{\mathrm{s}}+\mathbf{w})J\,\mathrm{d}V = 0 \tag{18}$$

$$\int_\Omega \delta\eta\nabla\cdot(\mathbf{j}^+-\mathbf{j}^-)J\,\mathrm{d}V = 0 \tag{19}$$

DOI: 10.1002/nme

where $\mathbf{E}^s$ and $\mathbf{S}^s_E$ are the Green–Lagrange strain of the solid phase and the second Piola–Kirchhoff stress due to solid deformation, respectively; $J=\det\mathbf{F}^s$ is the determinant of the solid phase deformation gradient tensor $\mathbf{F}^s$ and represents the volume change of a unit volume during deformation; and $\mathbf{n}$ is the outward normal unit vector of the surface. In basically the same manner as in the authors' previous work [12], the non-linear system of Equations (14)–(19) can be solved after discretization by applying the Newton–Raphson method with nodal displacement of the tissue, fluid flux, molar cation and anion fluxes, hydrostatic pressure and electrical potential as independent variables.

3. FINITE ELEMENT FORMULATION FOR CONTACT PROBLEMS OF CHARGED-HYDRATED SOFT TISSUES

3.1. Contact boundary conditions

As a part of the surface domain, boundary conditions also exist in the contact area. The special feature that distinguishes the contact boundary from the other boundaries is that the contact areas are unknown *a priori*, and boundary conditions in the contact area cannot be imposed arbitrarily since they have to obey mechanical and electrochemical principles and the mass conservation law for each phase during deformation to ensure proper mechanical and electrochemical load transfers and mass transfer between the contacting bodies. The contact boundary conditions are also referred to as the jump conditions since they are given across the boundary interface.

Figure 1 shows a contact system between two bodies. Considering that the point $\mathbf{x}^2$ of body 2 comes into contact with the point $\mathbf{x}^1$ of body 1, which is defined as the projection of $\mathbf{x}^2$ onto the surface of body 1, the penetration between the contact surfaces is defined as follows:

$$g=(\mathbf{x}^2-\mathbf{x}^1)\cdot\mathbf{n}^1 \tag{20}$$

As the frictional force can, in general, be determined from the contact pressure by introducing a suitable friction law, the friction force, i.e. the tangential component of the contact force, is omitted in this paper for the sake of simplicity. Thus, the contact forces can be expressed as

$$\mathbf{f}^1_c=\bar{t}^1\mathbf{n}^1,\quad \mathbf{f}^2_c=\bar{t}^2\mathbf{n}^2,\quad \mathbf{f}^1_c=-\mathbf{f}^2_c=\bar{t}\mathbf{n}^1 \tag{21}$$

by applying the relationship between the outward unit normal vectors in both the contact surfaces:

$$\mathbf{n}^1=-\mathbf{n}^2 \tag{22}$$

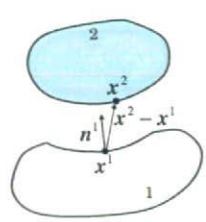

Figure 1. Contact system between two bodies.

DOI: 10.1002/nme

and the definition of contact pressure:

$$\bar{t} \equiv \bar{t}^1 = \bar{t}^2 \tag{23}$$

From the requirements of non-penetration and the compressive contact force, the geometric and kinetic constraint conditions between the contacting surfaces are given as:

$$g \geqslant 0, \quad \bar{t} \leqslant 0, \quad g \cdot \bar{t} = 0 \tag{24}$$

By applying the Reynolds transport theorem to the integral form of the mass, linear momentum and energy conservation laws [40], the following jump conditions, having a different but equivalent form to the original ones for convenience in the following formulation, were derived by Ateshian *et al.* [39] for triphasic problems:

$$\mu_c^{\mathrm{w},1} = \mu_c^{\mathrm{w},2}, \quad \tilde{\mu}_c^{+,1} = \tilde{\mu}_c^{+,2}, \quad \tilde{\mu}_c^{-,1} = \tilde{\mu}_c^{-,2} \tag{25}$$

$$(\mathbf{w}^1 - \mathbf{w}^2) \cdot \mathbf{n}^1 = 0, \quad (\mathbf{j}^{+,1} - \mathbf{j}^{+,2}) \cdot \mathbf{n}^1 = 0, \quad (\mathbf{j}^{-,1} - \mathbf{j}^{-,2}) \cdot \mathbf{n}^1 = 0 \tag{26}$$

The relationships in Equation (25) represent the chemical and electrochemical loads in the contact area, whereas the relationships in Equation (26) give the continuity conditions for inflow or outflow of the fluid and ionic phases, respectively.

As the contacting surfaces coincide with each other, the residual contact boundary conditions can be expressed on one side, say the surface of body 1, by substituting the relationships in Equations (21)–(23) and (25) into the right-hand side of Equations (14)–(17) in the contact area γ_c as

$$\begin{aligned} \delta R_c = & \int_{\gamma_c} (\delta \mathbf{u}^1 - \delta \mathbf{u}^2) \cdot \bar{t} \mathbf{n}^1 \, \mathrm{d}s + \int_{\gamma_c} (\delta \mathbf{w}^1 - \delta \mathbf{w}^2) \cdot \mu^{\mathrm{w}} \mathbf{n}^1 \, \mathrm{d}s \\ & + \int_{\gamma_c} (\delta \mathbf{j}^{+,1} - \delta \mathbf{j}^{+,2}) \cdot \tilde{\mu}^{+} \mathbf{n}^1 \, \mathrm{d}s + \int_{\gamma_c} (\delta \mathbf{j}^{-,1} - \delta \mathbf{j}^{-,2}) \cdot \tilde{\mu}^{-} \mathbf{n}^1 \, \mathrm{d}s \end{aligned} \tag{27}$$

where μ^{w}, $\tilde{\mu}^{+}$ and $\tilde{\mu}^{-}$ denote the chemical and electrochemical potentials of the fluid and ionic phases in the contact area according to the relationship in Equation (25). If constraint conditions are introduced into Equations (20) and (26) by applying the Lagrange multiplier method, the residual constraint conditions are imposed on the master surface by:

$$\delta \bar{R}_c = \int_{\gamma_c} [\delta \bar{t} (\mathbf{u}^1 - \mathbf{u}^2) + \delta \mu^{\mathrm{w}} (\mathbf{w}^1 - \mathbf{w}^2) + \delta \tilde{\mu}^{+} (\mathbf{j}^{+,1} - \mathbf{j}^{+,2}) + \delta \tilde{\mu}^{-} (\mathbf{j}^{-,1} - \mathbf{j}^{-,2})] \cdot \mathbf{n}^1 \, \mathrm{d}s \tag{28}$$

It is clear that the contact pressure and the chemical and electrochemical potentials play the role of Lagrange multipliers.

3.2. Discretization of contact surfaces

For contact problems with large deformations due to relative sliding, it is difficult to keep the finite element meshes conformable between the contacting surfaces for the description of the contact state. Therefore, the so-called node-to-segment approach is widely used in contact analyses, since it allows arbitrary movement of the contact node on the contact element of the counterpart contact surface. As shown in Figure 2, the candidate contact surfaces are divided into contact elements. The surface of one side (slave surface) is restrained such that it is unable to penetrate the surface of

DOI: 10.1002/nme

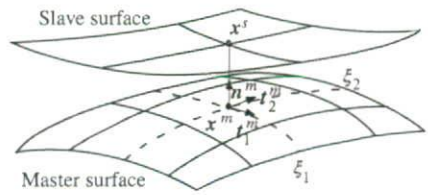

Figure 2. Discretization of contact surfaces.

the other side (master surface). Contact between node $\mathbf{x}^{\mathrm{s}}$ (slave node) in the slave surface and the element (master element) in the master surface is treated by means of determining the counterpart point $\mathbf{x}^{\mathrm{m}}$ (master point) of the slave node in the master surface by drawing a line perpendicular to the master element from the slave node.

In this way, it becomes possible to treat contact problems with a large amount of sliding between the contact surfaces by defining the geometric relationship between the node and the element, instead of that between nodes as in the node-to-node approach. In Figure 2, ξ^1 and ξ^2 indicate the convected coordinates at the master point $\mathbf{x}^{\mathrm{m}}$, while $\mathbf{t}_1^{\mathrm{m}}, \mathbf{t}_2^{\mathrm{m}}$ and $\mathbf{n}^{\mathrm{m}}$ are the covariant base vectors and outward unit normal vector, respectively:

$$\mathbf{t}_1^{\mathrm{m}} = \frac{\partial \mathbf{x}^{\mathrm{m}}}{\partial \xi^1}, \quad \mathbf{t}_2^{\mathrm{m}} = \frac{\partial \mathbf{x}^{\mathrm{m}}}{\partial \xi^2} \tag{29}$$

$$\mathbf{r}^{\mathrm{m}} \equiv \mathbf{t}_1^{\mathrm{m}} \times \mathbf{t}_2^{\mathrm{m}}, \quad \mathbf{n}^{\mathrm{m}} = \frac{\mathbf{r}^{\mathrm{m}}}{|\mathbf{r}^{\mathrm{m}}|} \tag{30}$$

Moreover, the differential area element in the convected coordinate system can be expressed as:

$$\mathrm{d}s = J^{\mathrm{m}}\,\mathrm{d}\xi^1\,\mathrm{d}\xi^2 = |\mathbf{r}^{\mathrm{m}}|\,\mathrm{d}\xi^1\,\mathrm{d}\xi^2 \tag{31}$$

By defining the shape function matrix with shape functions N_i^{m} $(i=1,n)$ of the contact element as

$$[P^{\mathrm{m}}] = \begin{bmatrix} N_1^{\mathrm{m}} & 0 & 0 & \cdots & N_n^{\mathrm{m}} & 0 & 0 \\ 0 & N_1^{\mathrm{m}} & 0 & \cdots & 0 & N_n^{\mathrm{m}} & 0 \\ 0 & 0 & N_1^{\mathrm{m}} & \cdots & 0 & 0 & N_n^{\mathrm{m}} \end{bmatrix} \tag{32}$$

the weight functions $\delta\mathbf{u}$, $\delta\mathbf{w}$, $\delta\mathbf{j}^+$, $\delta\mathbf{j}^-$, nodal displacement $\mathbf{u}^{\mathrm{m}}$ and location vector $\mathbf{x}^{\mathrm{m}}$ at the master point are interpolated as

$$\delta\mathbf{u}^{\mathrm{m}} = [P^{\mathrm{m}}]\{\delta u^{\mathrm{m}}\}, \quad \delta\mathbf{w}^{\mathrm{m}} = [P^{\mathrm{m}}]\{\delta w^{\mathrm{m}}\}, \quad \delta\mathbf{j}^{\alpha,\mathrm{m}} = [P^{\mathrm{m}}]\{\delta j^{\alpha,\mathrm{m}}\} \quad (\alpha = +,-) \tag{33}$$

$$\mathbf{u}^{\mathrm{m}} = [P^{\mathrm{m}}]\{u^{\mathrm{m}}\}, \quad \mathbf{x}^{\mathrm{m}} = [P^{\mathrm{m}}]\{x^{\mathrm{m}}\} \tag{34}$$

where

$$\{\delta u^{\mathrm{m}}\} = \{\delta u_{1,1}^{\mathrm{m}}, \delta u_{1,2}^{\mathrm{m}}, \delta u_{1,3}^{\mathrm{m}}, \ldots, \delta u_{n,1}^{\mathrm{m}}, \delta u_{n,2}^{\mathrm{m}}, \delta u_{n,3}^{\mathrm{m}}\}^{\mathrm{T}}$$

$$\{\delta w^{\mathrm{m}}\} = \{\delta w_{1,1}^{\mathrm{m}}, \delta w_{1,2}^{\mathrm{m}}, \delta w_{1,3}^{\mathrm{m}}, \ldots, \delta w_{n,1}^{\mathrm{m}}, \delta w_{n,2}^{\mathrm{m}}, \delta w_{n,3}^{\mathrm{m}}\}^{\mathrm{T}}$$

DOI: 10.1002/nme

$$\{\delta j^{\alpha,\mathrm{m}}\}=\{\delta j_{1,1}^{\alpha,\mathrm{m}},\delta j_{1,2}^{\alpha,\mathrm{m}},\delta j_{1,3}^{\alpha,\mathrm{m}},\ldots,\delta j_{n,1}^{\alpha,\mathrm{m}},\delta j_{n,2}^{\alpha,\mathrm{m}},\delta j_{n,3}^{\alpha,\mathrm{m}}\}^{\mathrm{T}}\quad(\alpha=+,-) \tag{35}$$

$$\begin{aligned}\{u^{\mathrm{m}}\}&=\{u_{1,1}^{\mathrm{m}}u_{1,2}^{\mathrm{m}},u_{1,3}^{\mathrm{m}},\ldots,u_{n,1}^{\mathrm{m}},u_{n,2}^{\mathrm{m}},u_{n,3}^{\mathrm{m}}\}^{\mathrm{T}}\\ \{x^{\mathrm{m}}\}&=\{x_{1,1}^{\mathrm{m}},x_{1,2}^{\mathrm{m}},x_{1,3}^{\mathrm{m}},\ldots,x_{n,1}^{\mathrm{m}},x_{n,2}^{\mathrm{m}},x_{n,3}^{\mathrm{m}}\}^{\mathrm{T}}\end{aligned} \tag{36}$$

are vectors consisting of the respective nodal values in the master element.

3.3. *Patch test*

The concept of the contact patch test in finite element structural analysis can be described as the ability to represent constant contact pressure in the contact area with a non-conforming mesh between the contact surfaces. Passing the contact patch test is a necessary condition for a contact analysis algorithm to ensure the convergence of the solution with mesh refinement. In the one-pass approach with the roles of master and slave surfaces, for example, the surface of body 1 in Figure 1 as the master and the surface of body 2 as the slave, fixed throughout the analysis, after finite element discretization, the discretized form of Equation (27) is represented for the master element and the assembly for all master element leads as:

$$\begin{aligned}\delta R_c=&\sum_e\int_{\gamma_m^e}(\delta\mathbf{u}^{\mathrm{m}}-\delta\mathbf{u}^{\mathrm{s}})\cdot\bar{t}\mathbf{n}^{\mathrm{m}}\,\mathrm{d}s+\sum_e\int_{\gamma_m^e}(\delta\mathbf{w}^{\mathrm{m}}-\delta\mathbf{w}^{\mathrm{s}})\cdot\mu^{\mathrm{w}}\mathbf{n}^{\mathrm{m}}\,\mathrm{d}s\\&+\sum_e\int_{\gamma_m^e}(\delta\mathbf{j}^{+,\mathrm{m}}-\delta\mathbf{j}^{+,\mathrm{s}})\cdot\tilde{\mu}^{+}\mathbf{n}^{\mathrm{m}}\,\mathrm{d}s+\sum_e\int_{\gamma_m^e}(\delta\mathbf{j}^{-,\mathrm{m}}-\delta\mathbf{j}^{-,\mathrm{s}})\cdot\tilde{\mu}^{-}\mathbf{n}^{\mathrm{m}}\,\mathrm{d}s\end{aligned} \tag{37}$$

Similarly, the discretized form of Equation (28) is given for the master elements as:

$$\delta\bar{R}_c=\sum_e\int_{\gamma_m^e}[\delta\bar{t}(\mathbf{u}^{\mathrm{m}}-\mathbf{u}^{\mathrm{s}})+\delta\mu^{\mathrm{w}}(\mathbf{w}^{\mathrm{m}}-\mathbf{w}^{\mathrm{s}})+\delta\tilde{\mu}^{+}(\mathbf{j}^{+,\mathrm{m}}-\mathbf{j}^{+,s})+\delta\tilde{\mu}^{-}(\mathbf{j}^{-,\mathrm{m}}-\mathbf{j}^{-,\mathrm{s}})]\cdot\mathbf{n}^{\mathrm{m}}\,\mathrm{d}s \tag{38}$$

As the assumption that the contact surfaces coincide with each other has been introduced in the derivation of Equation (27), Equation (37) only holds if the master and slave elements still coincide with each other. However, it is clear that this condition is no longer met in the case of non-conforming meshes. To bypass this obstacle in the conventional approach of structural analyses, approximations have been made by applying a concentrated contact force, instead of contact pressure, at the slave node or quadrature point of the slave element. However, since such an approximation is not, in general, consistent with the original contact boundary conditions of Equation (27), the contact patch test will not be satisfied and the resulting error cannot be improved by mesh refinement [41]. It is critical for a contact analysis algorithm of charged-hydrated soft tissues to pass the patch test, since not only errors in the contact pressure of the tissues, but also errors in the chemical and electrochemical potentials of the fluid and ionic phases and thus disturbed flow of the fluid and ions will be induced if the patch test is not satisfied.

To overcome this problem, a structural contact analysis algorithm that passes the patch test proposed by the authors [42] is extended to contact analysis of charged-hydrated soft tissues as follows. In contrast to the conventional approach, by performing integrations in the residual contact boundary conditions over all the contact elements of both the master and slave surfaces,

DOI: 10.1002/nme

the discretized form of the residual contact boundary conditions becomes:

$$\delta R_c = \sum_{e}^{\text{master}} \int_{\gamma_m^e} (\delta \mathbf{u}^{\mathrm{m}} \cdot \bar{t}^{\mathrm{m}} \mathbf{n}^{\mathrm{m}} + \delta \mathbf{w}^{\mathrm{m}} \cdot \mu^{\mathrm{w,m}} \mathbf{n}^{\mathrm{m}} + \delta \mathbf{j}^{+,\mathrm{m}} \cdot \tilde{\mu}^{+,\mathrm{m}} \mathbf{n}^{\mathrm{m}} + \delta \mathbf{j}^{-,\mathrm{m}} \cdot \tilde{\mu}^{-,\mathrm{m}} \mathbf{n}^{\mathrm{m}}) \, \mathrm{d}s$$

$$+ \sum_{e}^{\text{slave}} \int_{\gamma_s^e} (\delta \mathbf{u}^{\mathrm{s}} \cdot \bar{t}^{\mathrm{s}} \mathbf{n}^{\mathrm{s}} + \delta \mathbf{w}^{\mathrm{s}} \cdot \mu^{\mathrm{w,s}} \mathbf{n}^{\mathrm{s}} + \delta \mathbf{j}^{+,\mathrm{s}} \cdot \tilde{\mu}^{+,\mathrm{s}} \mathbf{n}^{\mathrm{s}} + \delta \mathbf{j}^{-,\mathrm{s}} \cdot \tilde{\mu}^{-,\mathrm{s}} \mathbf{n}^{\mathrm{s}}) \, \mathrm{d}s \tag{39}$$

In this way, the integrations can be evaluated regardless of the mesh configuration in the contact boundary. As a consequence, however, the nodal contact pressure and the chemical and electrochemical potentials of the fluid and ionic phases in the slave surface are involved in Equation (39) as additional nodal variables. This implies that contact constraints have to be imposed on the slave surface in addition to those on the master surface as in Equation (38). In structural contact analyses, overconstraint and resulting instability of the contact analysis have been indicated in the two-pass approach by imposing a non-penetration constraint on both the slave and master surfaces [41]. To eliminate the additional variables, the idea is to replace the nodal variables in the master element with those in the slave element by projecting the master nodes onto the slave elements as follows. The variables at any point within the master element can be interpolated by shape functions and their nodal values of the element as

$$\begin{aligned} \bar{t}^{\mathrm{m}} &= \{Q^{\mathrm{m}}\}^{\mathrm{T}} \{\bar{t}^{\mathrm{m}}\}, \quad \mu^{\mathrm{w,m}} = \{Q^{\mathrm{m}}\}^{\mathrm{T}} \{\mu^{\mathrm{w,m}}\} \\ \tilde{\mu}^{+,\mathrm{m}} &= \{Q^{\mathrm{m}}\}^{\mathrm{T}} \{\tilde{\mu}^{+,\mathrm{m}}\}, \quad \tilde{\mu}^{-,\mathrm{m}} = \{Q^{\mathrm{m}}\}^{\mathrm{T}} \{\tilde{\mu}^{-,\mathrm{m}}\} \end{aligned} \tag{40}$$

where:

$$\begin{aligned} \{Q^{\mathrm{m}}\}^{\mathrm{T}} &= \{M_1^{\mathrm{m}} \;\; M_2^{\mathrm{m}} \;\; \ldots \;\; M_k^{\mathrm{m}}\}, \quad \{\bar{t}^{\mathrm{m}}\}^{\mathrm{T}} = \{\bar{t}_1^{\mathrm{m}} \;\; \bar{t}_2^{\mathrm{m}} \ldots \;\; \bar{t}_k^{\mathrm{m}}\} \\ \{\mu^{\mathrm{w,m}}\}^{\mathrm{T}} &= \{\mu_1^{\mathrm{w,m}} \;\; \mu_2^{\mathrm{w,m}} \ldots \;\; \mu_k^{\mathrm{w,m}}\}, \quad \{\tilde{\mu}^{+,\mathrm{m}}\}^{\mathrm{T}} = \{\tilde{\mu}^{+,\mathrm{m}}\}^{\mathrm{T}} = \{\tilde{\mu}_1^{+,\mathrm{m}} \;\; \tilde{\mu}_2^{+,\mathrm{m}} \;\; \ldots \;\; \tilde{\mu}_k^{+,\mathrm{m}}\} \\ \{\tilde{\mu}^{-,\mathrm{m}}\}^{\mathrm{T}} &= \{\tilde{\mu}_1^{-,\mathrm{m}} \;\; \tilde{\mu}_2^{-,\mathrm{m}} \;\; \ldots \;\; \tilde{\mu}_k^{-,\mathrm{m}}\} \end{aligned} \tag{41}$$

The nodal variables at the master node are considered to be equal to the variables at the projected point in the slave element, which can be interpolated from the shape functions and the nodal variables of the projected slave element defined in the following:

$$\begin{aligned} \bar{t}_i^{\mathrm{m}} &= \{Q^{\mathrm{s}}\}_i^{\mathrm{T}} \{\bar{t}^{\mathrm{s}}\}_i, \quad \mu_i^{\mathrm{w,m}} = \{Q^{\mathrm{s}}\}_i^{\mathrm{T}} \{\mu^{\mathrm{w,s}}\}_i \\ \tilde{\mu}_i^{+,\mathrm{m}} &= \{Q^{\mathrm{s}}\}_i^{\mathrm{T}} \{\tilde{\mu}^{+,\mathrm{s}}\}_i, \quad \tilde{\mu}_i^{-,\mathrm{m}} = \{Q^{\mathrm{s}}\}_i^{\mathrm{T}} \{\tilde{\mu}^{-,\mathrm{s}}\}_i \end{aligned} \tag{42}$$

$$\begin{aligned} \{Q^{\mathrm{s}}\}_i^{\mathrm{T}} &= \{M_1^{\mathrm{s}} \;\; M_2^{\mathrm{s}} \;\; \ldots \;\; M_k^{\mathrm{s}}\}_i, \quad \{\bar{t}^{\mathrm{s}}\}_i^{\mathrm{T}} = \{\bar{t}_1^{\mathrm{s}} \;\; \bar{t}_2^{\mathrm{s}} \;\; \ldots \;\; \bar{t}_k^{\mathrm{s}}\}_i \\ \{\mu^{\mathrm{w,s}}\}_i^{\mathrm{T}} &= \{\mu_1^{\mathrm{w,s}} \;\; \mu_2^{\mathrm{w,s}} \;\; \ldots \;\; \mu_k^{\mathrm{w,s}}\}_i, \quad \{\tilde{\mu}^{+,\mathrm{s}}\}_i^{\mathrm{T}} = \{\tilde{\mu}_1^{+,\mathrm{s}} \;\; \tilde{\mu}_2^{+,\mathrm{s}} \;\; \ldots \;\; \tilde{\mu}_k^{+,\mathrm{s}}\}_i \\ \{\tilde{\mu}^{-,\mathrm{s}}\}_i^{\mathrm{T}} &= \{\tilde{\mu}_1^{-,\mathrm{s}} \;\; \tilde{\mu}_2^{-,\mathrm{s}} \;\; \ldots \;\; \tilde{\mu}_k^{-,\mathrm{s}}\}_i \end{aligned} \tag{43}$$

where the right subscript i of the matrices denotes that the shape function and nodal variables of the slave element are related to the nodal variables at the ith node of the master element. Consequently, the variables at any point within the master element are expressed as:

$$\begin{aligned} \bar{t}^{\mathrm{m}} &= \{L\}_m^{\mathrm{T}} \{\bar{t}^{\mathrm{s}}\}, \quad \mu^{\mathrm{w,m}} = \{L\}_m^{\mathrm{T}} \{\mu^{\mathrm{w,s}}\} \\ \tilde{\mu}^{+,\mathrm{m}} &= \{L\}_m^{\mathrm{T}} \{\tilde{\mu}^{+,\mathrm{s}}\}, \quad \tilde{\mu}^{-,\mathrm{m}} = \{L\}_m^{\mathrm{T}} \{\tilde{\mu}^{-,\mathrm{s}}\} \end{aligned} \tag{44}$$

DOI: 10.1002/nme

where

$$
\begin{aligned}
\{L\}^{\mathrm{T}} &= \{M_1^{\mathrm{m}}\{Q^{\mathrm{s}}\}_1^{\mathrm{T}} \;\; M_2^{\mathrm{m}}\{Q^{\mathrm{s}}\}_2^{\mathrm{T}} \;\; \dots \;\; M_k^{\mathrm{m}}\{Q^{\mathrm{s}}\}_k^{\mathrm{T}}\} \\
{}_m\{\bar{t}^{\mathrm{s}}\}^{\mathrm{T}} &= \{\{\bar{t}^{\mathrm{s}}\}_1^{\mathrm{T}} \;\; \{\bar{t}^{\mathrm{s}}\}_2^{\mathrm{T}} \;\; \dots \;\; \{\bar{t}^{\mathrm{s}}\}_k^{\mathrm{T}}\} \\
{}_m\{\mu^{\mathrm{w,s}}\}^{\mathrm{T}} &= \{\{\mu^{\mathrm{w,s}}\}_1^{\mathrm{T}} \;\; \{\mu^{\mathrm{w,s}}\}_2^{\mathrm{T}} \;\; \dots \;\; \{\mu^{\mathrm{w,s}}\}_k^{\mathrm{T}}\} \\
{}_m\{\tilde{\mu}^{+,\mathrm{s}}\}^{\mathrm{T}} &= \{\{\tilde{\mu}^{+,\mathrm{s}}\}_1^{\mathrm{T}} \;\; \{\tilde{\mu}^{+,\mathrm{s}}\}_2^{\mathrm{T}} \;\; \dots \;\; \{\tilde{\mu}^{+,\mathrm{s}}\}_k^{\mathrm{T}}\} \\
{}_m\{\tilde{\mu}^{-,\mathrm{s}}\}^{\mathrm{T}} &= \{\{\tilde{\mu}^{-,\mathrm{s}}\}_1^{\mathrm{T}} \;\; \{\tilde{\mu}^{-,\mathrm{s}}\}_2^{\mathrm{T}} \;\; \dots \;\; \{\tilde{\mu}^{-,\mathrm{s}}\}_k^{\mathrm{T}}\}
\end{aligned}
\tag{45}
$$

In the above matrices, the left subscript m of the matrices denotes the relationships of the slave nodal variables to the mth master element. By assembling all the contact elements of the master surface, all degrees of freedom regarding the variables of the master nodes are replaced by those of the slave nodes. Thus, only the variables of the slave nodes are retained and overconstraint can be avoided since only constraints for the slave nodes have to be imposed, as is the case for the conventional one-pass approach.

3.4. Discretized equation system of contact problems

Within the framework of finite element methods, variables at any point of an element are interpolated by shape functions using the nodal values. Thus, the residual contact boundary conditions in Equation (39) can be rewritten as

$$
\begin{aligned}
\delta R_c = \sum_e^{\text{master}} \int_{\gamma_m^e} & (\{\delta u^{\mathrm{m}}\}^{\mathrm{T}}[P^{\mathrm{m}}]^{\mathrm{T}}\{n^{\mathrm{m}}\}\{L\}^{\mathrm{T}}{}_m\{\bar{t}^{\mathrm{s}}\} + \{\delta w^{\mathrm{m}}\}^{\mathrm{T}}[P^{\mathrm{m}}]^{\mathrm{T}}\{n^{\mathrm{m}}\}\{L\}_m^{\mathrm{T}}\{\mu^{\mathrm{w,s}}\} \\
& + \{\delta j^{+,\mathrm{m}}\}^{\mathrm{T}}[P^{\mathrm{m}}]^{\mathrm{T}}\{n^{\mathrm{m}}\}\{L\}^{\mathrm{T}}{}_m\{\tilde{\mu}^{+,\mathrm{s}}\} + \{\delta j^{-,\mathrm{m}}\}^{\mathrm{T}}[P^{\mathrm{m}}]^{\mathrm{T}}\{n^{\mathrm{m}}\}\{L\}_m^{\mathrm{T}}\{\tilde{\mu}^{-,\mathrm{s}}\})\,\mathrm{d}s \\
& + \sum_e^{\text{slave}} \int_{\gamma_s^e} (\{\delta u^{\mathrm{s}}\}^{\mathrm{T}}[P^{\mathrm{s}}]^{\mathrm{T}}\{n^{\mathrm{s}}\}\{Q^{\mathrm{s}}\}^{\mathrm{T}}\{\bar{t}^{\mathrm{s}}\} + \{\delta w^{\mathrm{s}}\}^{\mathrm{T}}[P^{\mathrm{s}}]^{\mathrm{T}}\{n^{\mathrm{s}}\}\{Q^{\mathrm{s}}\}^{\mathrm{T}}\{\mu^{\mathrm{w,s}}\} \\
& + \{\delta j^{+,\mathrm{s}}\}^{\mathrm{T}}[P^{\mathrm{s}}]^{\mathrm{T}}\{n^{\mathrm{s}}\}\{Q^{\mathrm{s}}\}^{\mathrm{T}}\{\tilde{\mu}^{+,\mathrm{s}}\} + \{\delta j^{-,\mathrm{s}}\}^{\mathrm{T}}[P^{\mathrm{s}}]^{\mathrm{T}}\{n^{\mathrm{s}}\}\{Q^{\mathrm{s}}\}^{\mathrm{T}}\{\tilde{\mu}^{-,\mathrm{s}}\})\,\mathrm{d}s
\end{aligned}
\tag{46}
$$

where the definitions in Equations (32)–(33) and (35) are applied to the weight functions of both the master and slave elements, and the definitions in Equations (44)–(45) are applied to the Lagrange multipliers of the master element, which are related to the slave nodes. In addition, an interpolation similar to Equation (40) is applied to the Lagrange multipliers in the slave element. The matrix forms of the normal vectors $\mathbf{n}^{\mathrm{m}}$ and $\mathbf{n}^{\mathrm{s}}$ are denoted by $\{n^{\mathrm{m}}\}$ and $\{n^{\mathrm{s}}\}$. Although it is not a topic of this paper, it should be mentioned that selecting proper interpolations to satisfy the inf–sup condition is another crucial issue for ensuring the stability and optimal convergence of contact analyses of hydrated tissues.

The geometric constraint and continuity conditions of the fluid and ionic phases can be imposed on the slave node contacting the master element as shown in Figure 2. The residual boundary

DOI: 10.1002/nme

constraints of Equation (38) are discretized as

$$\begin{aligned}\delta\bar{R}_c = \sum_e \int_{\gamma_m^e} (&\{\delta\bar{t}\}^{\mathrm{T}}\{Q^{\mathrm{m}}\}\{n^{\mathrm{m}}\}([P^{\mathrm{m}}]\{u^{\mathrm{m}}\}-[I]\{u^{\mathrm{s}}\})+\{\delta\mu^{\mathrm{w}}\}^{\mathrm{T}}\{Q^{\mathrm{m}}\}\{n^{\mathrm{m}}\}\\ &\times([P^{\mathrm{m}}]\{w^{\mathrm{m}}\}-[I]\{w^{\mathrm{s}}\})+\{\delta\tilde{\mu}^{+}\}^{\mathrm{T}}\{Q^{\mathrm{m}}\}\{n^{\mathrm{m}}\}([P^{\mathrm{m}}]\{j^{+,\mathrm{m}}\}-[I]\{j^{+,\mathrm{s}}\})\\ &+\{\delta\tilde{\mu}^{-}\}^{\mathrm{T}}\{Q^{\mathrm{m}}\}\{n^{\mathrm{m}}\}([P^{\mathrm{m}}]\{j^{-,\mathrm{m}}\}-[I]\{j^{-,\mathrm{s}}\}))\,\mathrm{d}s\end{aligned} \tag{47}$$

based on the interpolations defined in Equations (32), (34) and (36), and similar definitions to the fluxes of the fluid and ionic phases. In addition, the interpolations for the Lagrange multipliers are defined in a similar manner to Equation (40).

Furthermore, by defining the equivalent nodal loads as

$$\begin{aligned}\{f_u^{\mathrm{m}}\} &= [P^{\mathrm{m}}]^{\mathrm{T}}\{n^{\mathrm{m}}\}\{L\}_m^{\mathrm{T}}\{\bar{t}^{\mathrm{s}}\}, \quad \{f_w^{\mathrm{m}}\}=[P^{\mathrm{m}}]^{\mathrm{T}}\{n^{\mathrm{m}}\}\{L\}^{\mathrm{T}}{}_m\{\mu^{\mathrm{w,s}}\}\\ \{f_{j^+}^{\mathrm{m}}\} &= [P^{\mathrm{m}}]^{\mathrm{T}}\{n^{\mathrm{m}}\}\{L\}^{\mathrm{T}}{}_m\{\tilde{\mu}^{+,\mathrm{s}}\}, \quad \{f_{j^-}^{\mathrm{m}}\}=[P^{\mathrm{m}}]^{\mathrm{T}}\{n^{\mathrm{m}}\}\{L\}^{\mathrm{T}}{}_m\{\tilde{\mu}^{-,\mathrm{s}}\}\\ \{f_u^{\mathrm{s}}\} &= [P^{\mathrm{s}}]^{\mathrm{T}}\{n^{\mathrm{s}}\}\{Q^{\mathrm{s}}\}^{\mathrm{T}}\{\bar{t}^{\mathrm{s}}\}, \quad \{f_w^{\mathrm{s}}\}=[P^{\mathrm{s}}]^{\mathrm{T}}\{n^{\mathrm{s}}\}\{Q^{\mathrm{s}}\}^{\mathrm{T}}\{\mu^{\mathrm{w,s}}\}\\ \{f_{j^+}^{\mathrm{s}}\} &= [P^{\mathrm{s}}]^{\mathrm{T}}\{n^{\mathrm{s}}\}\{Q^{\mathrm{s}}\}^{\mathrm{T}}\{\tilde{\mu}^{+,\mathrm{s}}\}, \quad \{f_{j^-}^{\mathrm{s}}\}=[P^{\mathrm{s}}]^{\mathrm{T}}\{n^{\mathrm{s}}\}\{Q^{\mathrm{s}}\}^{\mathrm{T}}\{\tilde{\mu}^{-,\mathrm{s}}\}\end{aligned} \tag{48}$$

and the nodal constraints as

$$\begin{aligned}\{g_u\} &= \{Q^{\mathrm{m}}\}\{n^{\mathrm{m}}\}([P^{\mathrm{m}}]\{u^{\mathrm{m}}\}-[I]\{u^{\mathrm{s}}\}), \quad \{g_w\}=\{Q^{\mathrm{m}}\}\{n^{\mathrm{m}}\}([P^{\mathrm{m}}]\{w^{\mathrm{m}}\}-[I]\{w^{\mathrm{s}}\})\\ \{g_{j^+}\} &= \{Q^{\mathrm{m}}\}\{n^{\mathrm{m}}\}([P^{\mathrm{m}}]\{j^{+,\mathrm{m}}\}-[I]\{j^{+,\mathrm{s}}\})\\ \{g_{j^-}\} &= \{Q^{\mathrm{m}}\}\{n^{\mathrm{m}}\}([P^{\mathrm{m}}]\{j^{-,\mathrm{m}}\}-[I]\{j^{-,\mathrm{s}}\})\end{aligned} \tag{49}$$

after numerical integration and assembly for all contact elements, Equations (46)–(47) can be rewritten as

$$\begin{aligned}\delta R_c = &\{\delta U^{\mathrm{m}}\}^{\mathrm{T}}\{F_u^{\mathrm{m}}\}+\{\delta W^{\mathrm{m}}\}^{\mathrm{T}}\{F_w^{\mathrm{m}}\}+\{\delta J^{+,\mathrm{m}}\}^{\mathrm{T}}\{F_{j^+}^{\mathrm{m}}\}+\{\delta J^{-,\mathrm{m}}\}^{\mathrm{T}}\{F_{j^-}^{\mathrm{m}}\}\\ &+\{\delta U^{\mathrm{s}}\}^{\mathrm{T}}\{F_u^{\mathrm{s}}\}+\{\delta W^{\mathrm{s}}\}^{\mathrm{T}}\{F_w^{\mathrm{s}}\}+\{\delta J^{+,\mathrm{s}}\}^{\mathrm{T}}\{F_{j^+}^{\mathrm{s}}\}+\{\delta J^{-,\mathrm{s}}\}^{\mathrm{T}}\{F_{j^-}^{\mathrm{s}}\}\end{aligned} \tag{50}$$

$$\delta\bar{R}_c=\{\delta\bar{T}\}^{\mathrm{T}}\{G_u\}+\{\delta M^{\mathrm{w}}\}^{\mathrm{T}}\{G_w\}+\{\delta\tilde{M}^{+}\}^{\mathrm{T}}\{G_{j^+}\}+\{\delta\tilde{M}^{-}\}^{\mathrm{T}}\{G_{j^-}\} \tag{51}$$

with the upper case character denoting the assembled vectors for all the contact elements.

For the whole contact system, by applying the finite element procedure presented in [12] to the governing equations of the triphasic theory, and further combining the resulting discretized forms of Equations (14)–(19) with Equations (50)–(51), the complete equation system for the whole contact system of the tissues can be derived with the Lagrange multipliers, i.e. the contact pressures, chemical potential of the fluid phase and electrochemical potentials of the cation and anion phases in the contact boundaries, as additional variables. With the contact stiffness matrices described in detail in the Appendix, the derived non-linear equations are solved using the Newton–Raphson method. The incremental matrix equation at the ith iteration has the form:

$$\left[\frac{K+K_{c1}K_{c2}}{K_{c3}}\right]^{(i)}\left\{\frac{\{\Delta\Gamma\}}{\{\Delta\Lambda\}}\right\}^{(i)}=\left\{\frac{\{\Delta F\}}{\{\Delta G\}}\right\}^{(i-1)} \tag{52}$$

DOI: 10.1002/nme

where

$$
\begin{aligned}
\{\Delta\Gamma\} &= \{\{\Delta U\}\ \{\Delta W\}\ \{\Delta J^{+}\}\ \{\Delta J^{-}\}\ \{\Delta P\}\ \{\Delta H\}\}^{\mathrm{T}} \\
\{\Delta\Lambda\} &= \{\{\Delta\bar{T}\}\ \{\Delta M^{w}\}\ \{\Delta\tilde{M}^{+}\}\ \{\Delta\tilde{M}^{-}\}\}^{\mathrm{T}} \\
\{\Delta F\}^{(i-1)} &= \{\{F_{\mathrm{ext}} - F_{u,\mathrm{int}}^{(i-1)}\}\ \{F_{w,\mathrm{ext}} - F_{w,\mathrm{int}}^{(i-1)}\}\ \{F_{j^{+},\mathrm{ext}} - F_{j^{+},\mathrm{int}}^{(i-1)}\}\ \{F_{j^{-},\mathrm{ext}} - F_{j^{-},\mathrm{int}}^{(i-1)}\}\}^{\mathrm{T}} \\
\{\Delta G\}^{(i-1)} &= \{\{-G_{u}^{(i-1)}\}\ \{-G_{w}^{(i-1)}\}\ \{-G_{j^{+}}^{(i-1)}\}\ \{-G_{j^{-}}^{(i-1)}\}\}^{\mathrm{T}}
\end{aligned}
\tag{53}
$$

with the following definitions: $\{\Delta U\}$, $\{\Delta W\}$, $\{\Delta J^{+}\}$, $\{\Delta J^{-}\}$, $\{\Delta P\}$ and $\{\Delta H\}$ represent the total vectors of incremental nodal displacement of the tissue, fluid flow, molar cation and anion flows, hydrostatic pressure and electric potential, respectively; $\{\Delta\bar{T}\}$, $\{\Delta M^{w}\}$, $\{\Delta\tilde{M}^{+}\}$ and $\{\Delta\tilde{M}^{-}\}$ denote the total vectors of the incremental nodal contact pressure, chemical potential of the fluid and electrochemical potentials of the cation and anion phases in the contact surfaces, respectively; $\{F_{\mathrm{ext}} - F_{u,\mathrm{int}}^{(i-1)}\}$, $\{F_{w,\mathrm{ext}} - F_{w,\mathrm{int}}^{(i-1)}\}$, $\{F_{j^{+},\mathrm{ext}} - F_{j^{+},\mathrm{int}}^{(i-1)}\}$ and $\{F_{j^{-},\mathrm{ext}} - F_{j^{-},\mathrm{int}}^{(i-1)}\}$ are the total vectors of the residual nodal force, chemical potential of fluid and electrochemical potentials of the cation and anion phases at the last iteration, respectively; and $\{-G_{u}^{(i-1)}\}$, $\{-G_{w}^{(i-1)}\}$, $\{-G_{j^{+}}^{(i-1)}\}$ and $\{-G_{j^{-}}^{(i-1)}\}$ give the total vectors of the residual nodal geometric constraint of the tissue and continuity constraints of the fluid and ionic phases at the last iteration, respectively. The contact stiffness matrices K_{c1}, K_{c2} and K_{c3} denote the assembled form of the stiffness matrices given in the Appendix. In addition, it should be noted that the nodal variables, except for the Lagrange multipliers in the contact surface, have been assembled to the relative degrees of freedom.

4. NUMERICAL EXAMPLES

The formulation performed in Section 3 is implemented by building the nodal contact pressure of the tissues, nodal fluxes of the fluid and ionic phases and contact tangent stiffness associated with the contacting surfaces into a in-house triphasic finite element analysis program [12]. Next, numerical examples are carried out to assess the validity and effectiveness of the proposed approach using a hexahedral type of element with eight nodes for displacement and fluxes of the fluid and ionic phases, and one node for the hydrostatic pressure and electrical potential. The same interpolation functions are used for the displacement and fluxes of the fluid and ionic phases, and the Lagrange multipliers in the contact boundary. Typical values of the material properties of articular cartilage from the literature are adopted in these examples.

4.1. Stress relaxation in a confined problem

As no analytical solution of triphasic contact problems has been reported in the literature to the best of the authors' knowledge, the confined model shown in Figure 3 is used to test the continuity constraints by setting the mid-section as the contact interface. Assuming that the tissues are isotropic materials, the material parameters are selected based on those given in [43]: the negative fixed-charge density in equivalent moles per unit initial tissue volume $c_0^F = 0.2\,\mathrm{Eq/l}$; solid volume fraction before deformation $\phi_0^s = 0.25$; diffusion coefficients of the cation and anion phases $d^{+} = 0.5\times10^{-9}\,\mathrm{m^2/s}$ and $d^{-} = 0.8\times10^{-9}\,\mathrm{m^2/s}$, respectively; permeability $\kappa = 1.07\times10^{-15}\,\mathrm{m^4/(Ns)}$; and the activity and osmotic coefficients $\gamma^{\pm} = \gamma^{\pm *} = \Phi = 1.0$. Young's modulus and the Poisson ratio

DOI: 10.1002/nme

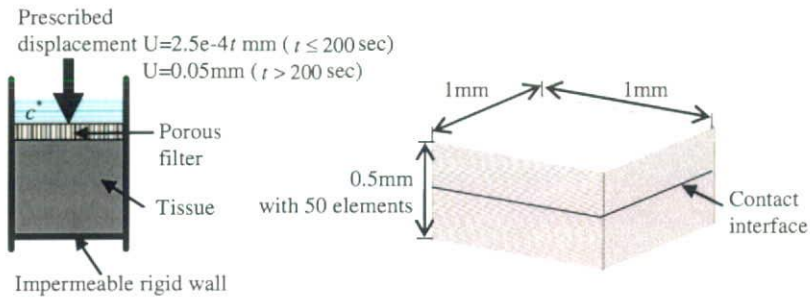

Figure 3. Confined contact model.

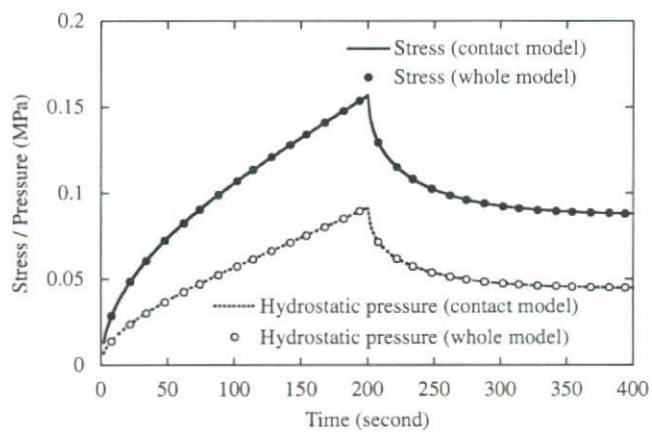

Figure 4. Comparison of the total stress and hydrostatic pressure histories at the upper surface obtained by the contact model and whole model.

of the tissues are set to be 0.3 MPa and 0.0, respectively. The external bath concentration c^* is 0.15 M NaCl at temperature $T = 298\,\mathrm{K}$, while the universal gas constant R is $8.314\,\mathrm{J/(mol\,K)}$. The total stress and hydrostatic pressure at the upper surface are compared with those obtained using the triphasic finite element analysis program verified in [12] for a confined model as a whole model. The good agreement between these results shown in Figure 4 indicates that the continuity constraints are well satisfied and that the mechanical and chemical loads are correctly transferred in the contact boundary.

4.2. Patch test

A crucial issue in contact analyses of charged-hydrated soft tissues is the contact patch test. The typical model shown in Figure 5, with the same material properties as those in Section 4.1, is used to confirm the ability of the present algorithm to pass the contact patch test. The depth in the Z-direction is 1 mm with one element. All degrees of freedom in the Z-direction are fixed. In the case of a single solid phase, it has been indicated in [41] that, for an applied uniform external load, the actual uniform contact pressure at the contact interface cannot be obtained from such a non-conforming mesh, since the contact patch test is not satisfied due to inconsistent discretization

DOI: 10.1002/nme

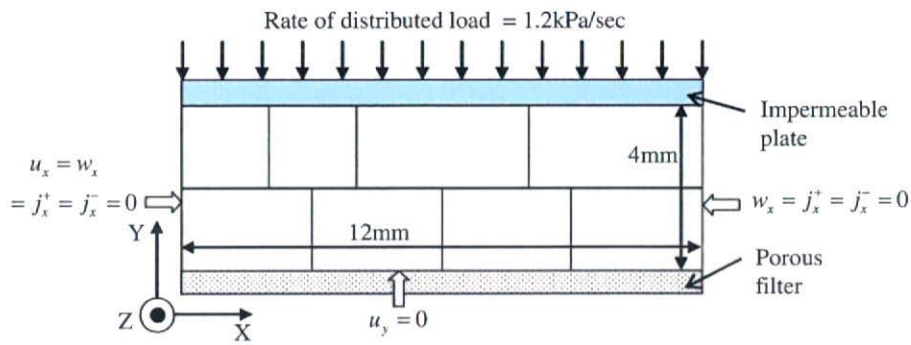

Figure 5. Patch test model.

of the contact virtual work. In contact analyses of charged-hydrated soft tissues, for a similar reason, it is anticipated that if the applied algorithm fails the patch test, the uniform chemical and electrochemical potentials of the fluid and ionic phases also cannot be obtained and unrealistic fluid and ion flows will be induced. However, remarkably uniform distributions of the contact pressure and the chemical and electrochemical potentials of the fluid and ionic phases are obtained by the proposed algorithm. The nodal contact pressures are precisely the same as the distributed load. Furthermore, the ability of the proposed algorithm to pass the contact patch test is also confirmed by the resulting uniform distribution of the fluid flux and ionic molar fluxes in the contact surface. For clarity, the straightforward figures of the results are omitted here.

4.3. Contact problem between articular cartilage layers

To further verify the effectiveness of the proposed algorithm, a contact analysis is performed for contacting articular cartilage layers with large sliding. The finite element mesh generated without special attention to the conformability and combination of element types between the contact surfaces is shown in Figure 6. All the nodal degrees of freedom of displacement, and fluid and ionic fluxes at the top of the upper cartilage layer and bottom of the lower cartilage layer are constrained by assuming that the cartilage layer is connected to an impermeable rigid bone. The nodal degrees of freedom of displacement, fluid flux and ionic fluxes in the outward direction of the plane are constrained to simulate a 2-D problem. The solid phase of the two cartilage layers is assumed to be a hyperelastic material of the Saint Venant–Kirchhoff type with the same material constants specified in Section 4.1.

The load is first linearly applied to 0.2 N within 0.002 s. Afterward, a reciprocating motion with a horizontal velocity of 10 mm/s, starting rightward, is applied to the upper cartilage to produce relative sliding over the lower cartilage within the zone shown in Figure 6, while the vertical load remains unchanged. Figure 7 shows the deformation of the cartilage layers together with the flow field of the fluid phase during the first half of the second cycle. Smooth deformation of the contact surface is observed and the fluid is squeezed remarkably near the edge of the contact interface. The flow field of the fluid phase inside the contact surface also has a smooth distribution as shown in Figure 8. Near the center of the contact surface, the fluid is squeezed from the lower cartilage into the upper cartilage, while, apart from the center, the fluid flows toward the edge of the contact interface.

DOI: 10.1002/nme

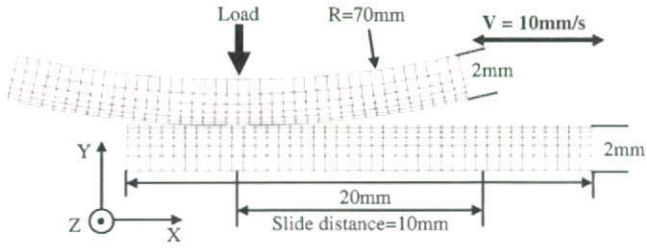

Figure 6. The FEM model of contacting cartilage layers.

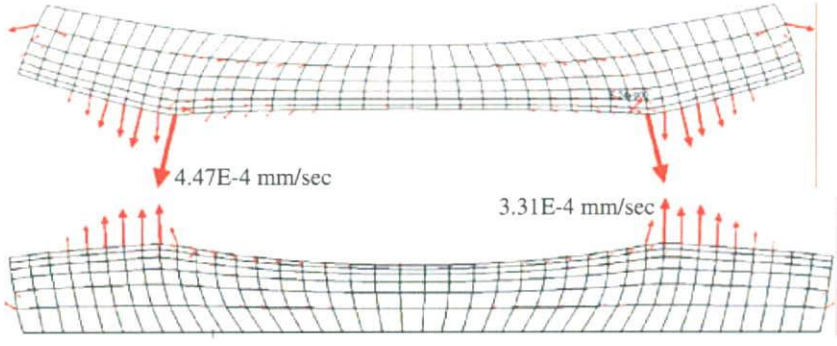

Figure 7. Deformation of the cartilage layers (amplified by 3) and flow field of the fluid phase.

The contact pressure, chemical potential of the fluid phase and electrochemical potential of the ionic phases present smooth distributions along the contact interface as shown in Figure 9, with the electrochemical potentials of the cation and anion phases normalized by the bath electrochemical potential. In addition, similar distributions are confirmed throughout the whole sliding history. Furthermore, even when a rather coarse mesh is used, the contour maps of the chemical potential of the fluid phase during the first half of the second cycle shown in Figure 10 give quite continuous distributions between the contacting cartilage layers. Although not shown here, similar results are also obtained for the ionic electrochemical potentials. From the above observations, it can be concluded that, with the ability to pass the contact patch test, the proposed algorithm exhibits a good performance for application to contact analyses of charged-hydrated soft tissues.

5. CONCLUSIONS

Contact phenomena with large sliding occur between articular cartilages when synovial joints function for load transfer during movement of the human body in daily life. On the other hand, as a charged-hydrated material, coupling between mechanical, electrical and chemical events is responsible for the complicated phenomena in articular cartilage. Thus, it is required to develop a contact analysis algorithm that takes coupling of mechanical and electrochemical behaviors into account while having the ability to treat large sliding. However, even for the originally generated conforming mesh, the conformance is lost during sliding between the contacting bodies. Therefore,

DOI: 10.1002/nme

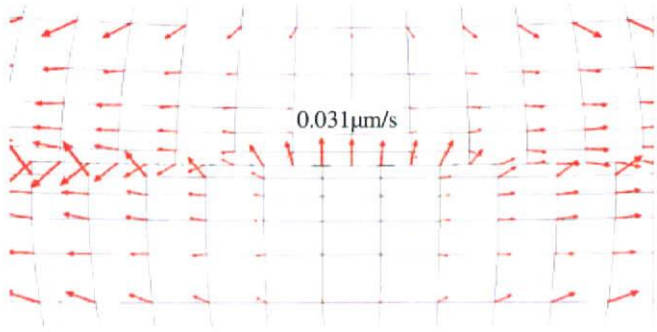

Figure 8. Flow field of the fluid phase near the center of the contact surface.

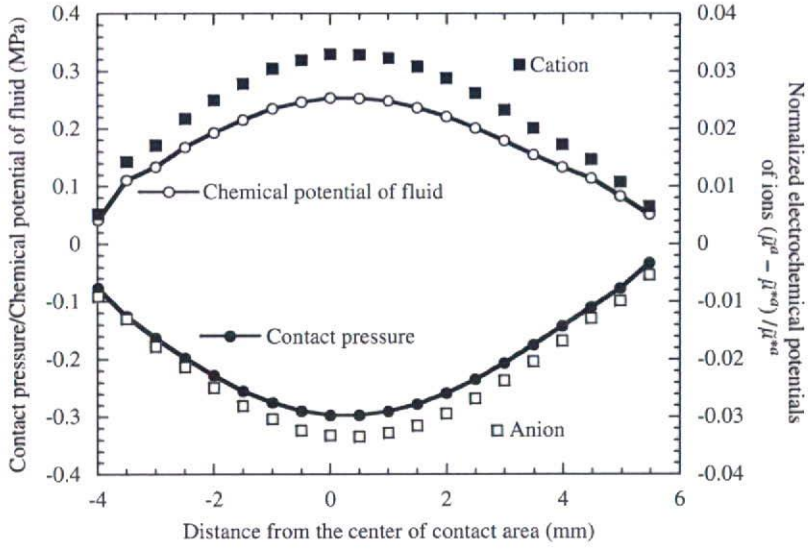

Figure 9. Distributions of the contact pressure, chemical potential of the fluid and electrochemical potential of ions within the contact area.

the contact patch test arises as an important issue for obtaining reasonable solutions of contact analyses. Failure in the contact patch test for such non-conformable meshes will induce errors of the contact pressure and the chemical and electrochemical potentials of the fluid and ionic phases, and further result in disturbance of the flow fields of the fluid and ionic phases. In this work, a finite element contact analysis approach for charged-hydrated soft tissues is proposed by imposing an impenetrability constraint of the bodies and continuity of the interstitial fluid and ion phases at the contact surfaces with introduction of the contact pressure, chemical potential of the fluid and electrochemical potentials of ions as Lagrange multipliers. The node-to-segment one-pass strategy is adopted to treat large sliding. In order to ensure consistent mechanical, chemical and electrochemical behaviors between the contacting bodies, the requirement of passing the contact patch test is satisfied by performing integration of the residual contact boundary conditions over

DOI: 10.1002/nme

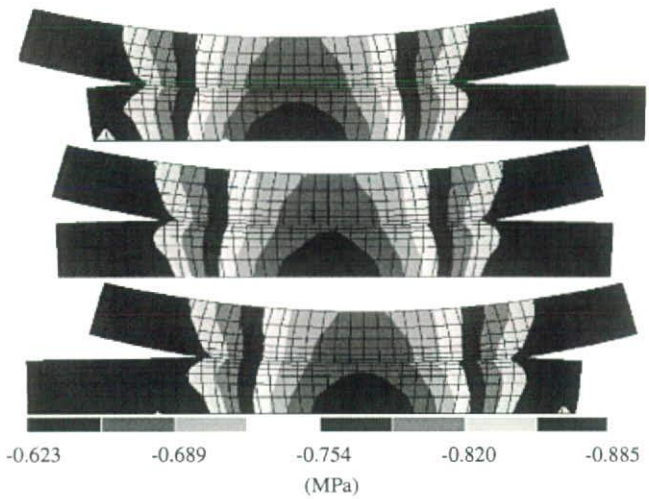

Figure 10. Contour maps of the chemical potential of the fluid phase during the first half of the second cycle.

both the master and slave contact surfaces. On the other hand, to avoid overconstraint, the nodal degrees of freedom of the master nodes are eliminated by transmitting the master nodal variables to the projected points at the slave surface, which are then interpolated from the nodal variables of the slave nodes. The proposed algorithm is verified by numerical examples. The obtained consistent flow fields of the fluid and ionic phases between the contacting bodies and the smooth distributions of the contact pressure, chemical potential of the fluid phase and electrochemical potentials of the ions within the contact area indicate good performance of the proposed algorithm. Although the frictional effect is not involved in the formulation, it is not difficult to introduce a frictional term as long as the frictional law is determined. Clinical application of this algorithm is the goal of our future work.

APPENDIX A

The tangential matrices regarding the contact boundary conditions are obtained as follows from differentiation of the equivalent nodal forces and nodal contact constraints with respect to the displacement of the tissues, fluxes of the fluid and ionic phases and the Lagrange multipliers:

$$\{\Delta F_u^\alpha\} = \frac{\partial\{F_u^\alpha\}}{\partial\{U^\alpha\}}\{\Delta U^\alpha\} + \frac{\partial\{F_u^\alpha\}}{\partial\{\bar{T}^s\}}\{\Delta\bar{T}^s\} = [K_{u,u}^\alpha]\{\Delta U^\alpha\} + [K_{u,\bar{t}^s}^\alpha]\{\Delta\bar{T}^s\} \tag{A1}$$

$$\{\Delta F_w^\alpha\} = \frac{\partial\{F_w^\alpha\}}{\partial\{U^\alpha\}}\{\Delta U^\alpha\} + \frac{\partial\{F_w^\alpha\}}{\partial\{M^{w,s}\}}\{\Delta M^{w,s}\} = [K_{w,u}^\alpha]\{\Delta U^\alpha\} + [K_{w,\mu^{w,s}}^\alpha]\{\Delta M^{w,s}\} \tag{A2}$$

$$\{\Delta F_{j^+}^\alpha\} = \frac{\partial\{F_{j^+}^\alpha\}}{\partial\{U^\alpha\}}\{\Delta U^\alpha\} + \frac{\partial\{F_{j^+}^\alpha\}}{\partial\{\tilde{M}^{+,s}\}}\{\Delta\tilde{M}^{+,s}\} = [K_{j^+,u}^\alpha]\{\Delta U^\alpha\} + [K_{j^+,\tilde{\mu}^{+,s}}^\alpha]\{\Delta\tilde{M}^{+,s}\} \tag{A3}$$

DOI: 10.1002/nme

$$\{\Delta F^{\alpha}_{j^-}\}=\frac{\partial\{F^{\alpha}_{j^-}\}}{\partial\{U^{\alpha}\}}\{\Delta U^{\alpha}\}+\frac{\partial\{F^{\alpha}_{j^-}\}}{\partial\{\tilde{M}^{-,\mathrm{s}}\}}\{\Delta\tilde{M}^{-,\mathrm{s}}\}=[K^{\alpha}_{j^-,u}]\{\Delta U^{\alpha}\}+[K^{\alpha}_{j^-,\tilde{\mu}^{-,\mathrm{s}}}]\{\Delta\tilde{M}^{-,\mathrm{s}}\} \tag{A4}$$

$$\{\Delta G_u\}=\frac{\partial\{G_u\}}{\partial\{U^{\mathrm{m}}\}}\{\Delta U^{\mathrm{m}}\}=[K_{G_u,u}]\{\Delta U^{\mathrm{m}}\} \tag{A5}$$

$$\{\Delta G_w\}=\frac{\partial\{G_w\}}{\partial\{U^{\mathrm{m}}\}}\{\Delta U^{\mathrm{m}}\}+\frac{\partial\{G_w\}}{\partial\{W^{\mathrm{m}}\}}\{\Delta W^{\mathrm{m}}\}=[K_{G_w,u}]\{\Delta U^{\mathrm{m}}\}+[K_{G_w,w}]\{\Delta W^{\mathrm{m}}\} \tag{A6}$$

$$\{\Delta G_{j^+}\}=\frac{\partial\{G_{j^+}\}}{\partial\{U^{\mathrm{m}}\}}\{\Delta U^{\mathrm{m}}\}+\frac{\partial\{G_{j^+}\}}{\partial\{J^{+,\mathrm{m}}\}}\{\Delta J^{+,\mathrm{m}}\}=[K_{G_{j^+},u}]\{\Delta U^{\mathrm{m}}\}+[K_{G_{j^+},j^+}]\{\Delta J^{+,\mathrm{m}}\} \tag{A7}$$

$$\{\Delta G_{j^-}\}=\frac{\partial\{G_{j^-}\}}{\partial\{U^{\mathrm{m}}\}}\{\Delta U^{\mathrm{m}}\}+\frac{\partial\{G_{j^-}\}}{\partial\{J^{-,\mathrm{m}}\}}\{\Delta J^{-,\mathrm{m}}\}=[K_{G_{j^-},u}]\{\Delta U^{\mathrm{m}}\}+[K_{G_{j^-},j^-}]\{\Delta J^{-,\mathrm{m}}\} \tag{A8}$$

where the superscript $\alpha=\mathrm{m},\mathrm{s}$ denotes the quantities in the master or slave surfaces, and the upper case character indicates the assembled nodal variables. By use of the following definitions:

$$[K^{\alpha}_{\Gamma,U}]=\begin{bmatrix}[K^{\alpha}_{u,u}] & [0] & [0] & [0]\\ [K^{\alpha}_{w,u}] & [0] & [0] & [0]\\ [K^{\alpha}_{j^+,u}] & [0] & [0] & [0]\\ [K^{\alpha}_{j^-,u}] & [0] & [0] & [0]\end{bmatrix}\quad(\alpha=\mathrm{m},\mathrm{s}) \tag{A9}$$

$$[K^{\alpha}_{\Gamma,\Lambda}]=\begin{bmatrix}[K^{\alpha}_{u,\tilde{t}^{\mathrm{s}}}] & [0] & [0] & [0]\\ [0] & [K^{\alpha}_{w,\mu^{\mathrm{w},\mathrm{s}}}] & [0] & [0]\\ [0] & [0] & [K^{\alpha}_{j^+,\tilde{\mu}^{+,\mathrm{s}}}] & [0]\\ [0] & [0] & [0] & [K^{\alpha}_{j^-,\tilde{\mu}^{-,\mathrm{s}}}]\end{bmatrix}\quad(\alpha=\mathrm{m},\mathrm{s}) \tag{A10}$$

$$[K^{\mathrm{m}}_{\Lambda,\Gamma}]=\begin{bmatrix}[K_{G_u,u}] & [0] & [0] & [0]\\ [K_{G_w,u}] & [K_{G_w,w}] & [0] & [0]\\ [K_{G_{j^+},u}] & [0] & [K_{G_{j^+},j^+}] & [0]\\ [K_{G_{j^-},u}] & [0] & [0] & [K_{G_{j^-},j^-}]\end{bmatrix} \tag{A11}$$

$$\{\Gamma^{\alpha}\}^{\mathrm{T}}=\{U^{\alpha},W^{\alpha},J^{+,\alpha},J^{-,\alpha}\}\quad(\alpha=\mathrm{m},\mathrm{s}) \tag{A12}$$

$$\{\Lambda\}^{\mathrm{T}}=\{\tilde{T},M^{\mathrm{w}},\tilde{M}^{+},\tilde{M}^{-}\} \tag{A13}$$

$$\{F^{\alpha}_{\Gamma}\}^{\mathrm{T}}=\{F^{\alpha}_{u},F^{\alpha}_{w},F^{\alpha}_{j^+},F^{\alpha}_{j^-}\}\quad(\alpha=\mathrm{m},\mathrm{s}) \tag{A14}$$

$$\{G_{\Lambda}\}^{\mathrm{T}}=\{G_u,G_w,G_{j^+},G_{j^-}\} \tag{A15}$$

DOI: 10.1002/nme